Anisotropy of the Fermi Surface of p-Type PbTe

J. Richard Burke, Bland Houston, and H. T. Savage
U. S. Naval Ordnance Laboratory, White Oak, Silver Spring, Maryland 20910
(Received 14 January 1970)

We have studied the angular dependence of Shubnikov–de Haas oscillations in a sample of p-type PbTe having a hole concentration of 3.0×10^{18} cm^{-3}. Orientations of the magnetic field in a {110} plane and temperatures between 4.2 and 1.2 °K were used. For the first time in this material, the component frequencies were determined by Fourier analysis. The angular dependence of the corresponding extremal areas was precisely fitted by four ⟨111⟩-oriented ellipsoids of revolution having a "mass anisotropy" of 13 and containing the same number of holes as that determined from the high-field Hall coefficient. These results, which are considerably different from those previously reported by Cuff *et al.* for material with the same hole concentration, suggest that the anisotropy is constant, at least up to the hole concentration studied here. A $\vec{k}\cdot\vec{p}$ band model, consistent with this behavior and with other results presented here, is considered. From the temperature dependence of the oscillations with $\vec{H}\parallel[111]$, the transverse effective mass at the Fermi level $m_\perp(\epsilon_F)$ is $(0.036\pm0.002)m$. Longitudinal and transverse effective g values at the Fermi level were determined from the spin splitting of peaks in the oscillations. For $\vec{H}\parallel[111]$, the ratio of spin splitting to Landau-level separation is 0.58 ± 0.01, and $g_\parallel(\epsilon_F)=32\pm2$. For $\vec{H}_\perp[111]$, this ratio is 0.27 ± 0.01, and $g_\perp(\epsilon_F)=7\pm2$.

I. INTRODUCTION

It is well known that the four extrema of the principal valence band of PbTe are located at the L points of the Brillouin zone of the fcc lattice.[1] Since PbTe is an extrinsic semiconductor with large mobilities, Fermi-surface studies by means of Shubnikov–de Haas[2–4] and de Haas–van Alphen[5] oscillations, Azbel'–Kaner cyclotron resonance,[6] and magnetoacoustic attenuation[7] have been carried out.

A study of the carrier-concentration dependence of the cyclotron effective mass and the Fermi-surface anisotropy near the top of the valence band was first reported by Cuff, Ellett, and Kuglin.[2,3] A similar study of the anisotropy has recently been completed by Schilz[7] on both p- and n-type material.

Cuff *et al.*[2,3] interpreted the observed increase in the transverse cyclotron mass with increasing carrier concentration in terms of the nonparabolic, nonellipsoidal model developed by Cohen[8] for bismuth. They also reported that the mass anisotropy decreased from approximately 13 for a hole concentration of about 4×10^{17} cm^{-3} to 6 for a concentration of 3×10^{18} cm^{-3}. This decrease is much larger than that predicted by the model and was accompanied by a corresponding decrease in the carrier count relative to that measured by the high-field Hall coefficient.[9] This suggested the possibility that some of the carriers had entered a second valence band, especially since carrier counts obtained by these two methods were in good agreement for the other lead salts.[9]

The purpose of this paper is to present results obtained on material having a concentration of 3.0×10^{18} cm^{-3} that show that the mass anisotropy at this concentration is 13, rather than the value 6 reported by Cuff *et al.*[2] An anisotropy of 13 corresponds to the volume in k space that precisely accounts for the total number of carriers we obtained from the high-field Hall coefficient. In the light of the similar value of anisotropy found by Cuff *et al.* at low hole concentrations, where all carriers were accounted for, our value suggests that the anisotropy is approximately constant, at least up to a hole concentration of 3.0×10^{18} cm^{-3}. Within experimental error, this is consistent both with the Cohen model and also with a more exact model for PbTe to be discussed.

As Dimmock and Wright[10] pointed out, one of the parameters most sensitive to the important band interactions that determine the properties of carriers at the Fermi energy is the ratio of spin-splitting to the Landau-level separation. The determination of this ratio is described in detail for the two principal orientations of the magnetic field $\vec{H}\parallel[111]$ and $\vec{H}\perp[111]$. From these ratios and the corresponding cyclotron effective masses, effective g values at the Fermi surface $g_\parallel(\epsilon_F)$ and $g_\perp(\epsilon_F)$ are obtained.

II. THEORY OF SHUBNIKOV–de HAAS EFFECT

There are a number of papers and review articles that describe the theory of electrical transport phenomena in the quantum regime.[11] For the oscillatory component of the resistivity, we will use a slight modification of the expression given by Roth and Argyres[11]:

$$\rho = A\rho_0 \sum_{r=1}^{\infty} b_r \cos[2\pi(rc\hbar S/2\pi e)H^{-1} - 2\pi r\gamma - \tfrac{1}{4}\pi], \quad (1)$$

where

$$b_r = \frac{1}{r^{1/2}}\left(\frac{\hbar\omega_c}{2\zeta}\right)^{1/2} \frac{(2\pi^2 rkT/\hbar\omega_c)e^{-2\pi r/\omega_c\tau}}{\sinh(2\pi^2 rkT/\hbar\omega_c)} \times \cos(\pi r m^{\rm cyc} g/2m) \ . \quad (2)$$

ρ_0 is the zero-field resistivity, and A is a constant which depends on the orientation of the magnetic field relative to the current direction. For a given orientation of the magnetic field, the extremal cross section S of the Fermi surface in k space perpendicular to the field determines the frequency of the fundamental oscillation ($r=1$). The amplitude factor b_r, which determines the damping of the oscillations as a function of field strength and temperature, also depends upon (i) the cyclotron frequency $\omega_c = eH/m^{\rm cyc}c$, where $m^{\rm cyc}$ is the cyclotron effective mass, (ii) the Fermi level ζ, (iii) the effective g value g, and (iv) the lifetime τ of the Landau states. Finally, m is the free-electron mass. The phase of a component oscillation at $1/H=0$ is determined by γ, which is equal to $\frac{1}{2}$ in the free-electron approximation, and by the term $\cos(\pi m^{\rm cyc} rg/2m)$.

The summation over r includes all harmonics of the fundamental frequency. If the Fermi surface is a single sheet having more than one extremal cross section, or if, as in the case of PbTe, there is more than one sheet, one should also include a summation over extremal cross sections in Eq. (1).

From the argument of the cosine in Eq. (1), the frequency of the fundamental oscillation ($r=1$) is

$$F = (c\hbar/2\pi e)\, S = (1.04 \times 10^{-8})S \ , \quad (3)$$

where the units of S are $\rm cm^{-2}$, and F is in G. For an ellipsoid of revolution, this can be written as

$$F = 3.15\times 10^5 (p/10^{18})^{2/3} K^{1/6}[1 + (K-1)\cos^2\Theta]^{-1/2}, \quad (4)$$

where p is the number of carriers enclosed, Θ is the angle between the direction of the magnetic field and the major axis, and K is the square of the maximum-to-minimum cross-section ratio.

III. EXPERIMENTAL

The sample measured was taken from a single crystal pulled by the Czochralski technique. It was annealed at 420 °C to obtain a hole concentration of about 3×10^{18} $\rm cm^{-3}$ and to improve the homogeneity. The improved homogeneity reduces spatial fluctuations in the Fermi level relative to the band edge and thus minimizes damping of the oscillations due to spatial variations in the extremal cross sections of the Fermi surface. The actual hole concentration was determined from a measurement of the high-field Hall coefficient which yielded a value of 3.0×10^{18} $\rm cm^{-3}$.

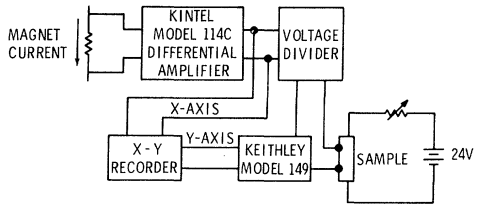

FIG. 1. Block diagram of the apparatus used to obtain x-y recorder traces of Shubnikov–de Haas oscillations. The signal from the voltage divider is used to buck out the background magnetoresistance.

The sample was mounted in a $\frac{3}{4}$-in. o.d. single-axis rotating holder for measurements in a $1\frac{1}{4}$-in.-bore 150-kG solenoid provided by the Naval Research Laboratory. Conventional dc measurement techniques were used. Figure 1 shows a block diagram of the apparatus. The signal from the voltage probes was of the order of 100 μV at 4.2 °K for a sample current of 400 mA. This signal was bucked by a fraction of the output from a Model 114 C Kintel differential amplifier. The imput for this amplifier was provided by the voltage drop across a resistor in the magnet current circuit. The bucking voltage, which is linear in the magnetic field, is necessary to reduce the large background magnetoresistance so that the Shubnikov–de Haas oscillations can be observed with greater sensitivity. The net signal was then fed to a Keithley Model 149 microvoltmeter. The output of the Keithley was displayed on the vertical axis of an x-y recorder whose horizontal axis was driven by the output of the Kintel amplifier. Traces of the Shubnikov–de Haas oscillations were then made for each sample orientation.

IV. RESULTS AND DISCUSSION

A. Angular Dependence of Extremal Cross Sections

All of the data to be described in this paper were obtained for crystallographic orientations of the magnetic field $\vec{H}$ in a $\{110\}$-type plane, which, to be specific, we take to be the $(1\bar{1}0)$ plane. Figure 2 shows this plane of rotation of the field relative to the four $\langle 111\rangle$-hole ellipsoids of PbTe. Figure 3 presents the oscillatory pattern obtained for an angle Θ between $\vec{H}$ and the [110] axis equal to 55°. The Fermi surface exhibits three extremal cross sections for this orientation, one of these corresponding to the largest of ellipsoid B. The corresponding oscillation is usually difficult to detect because of the large cyclotron mass for this orbit. In addition, an accurate determination of its frequency is complicated by the presence of the other

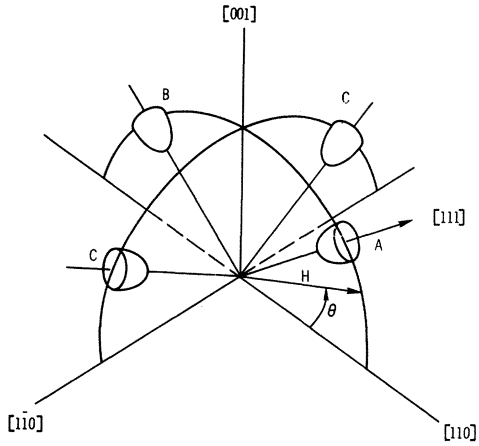

FIG. 2. Four ⟨111⟩ ellipsoids of p-type PbTe. Data were obtained for orientations of the magnetic field $\vec{H}$ in the plane of ellipsoids A and B.

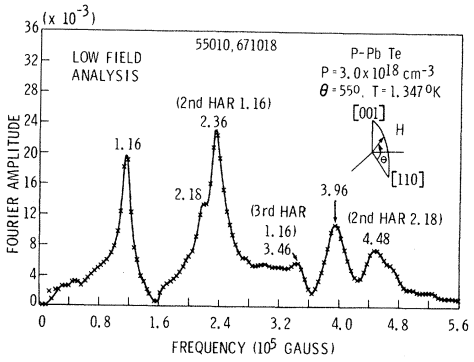

FIG. 4. Fourier analysis of the data in Fig. 3. The peak at 3.96×10^5 G corresponds to the largest extremal cross section of ellipsoid B. Those at 1.16 and 2.18 $\times10^5$ G correspond to the other two cross sections exhibited by ellipsoids A and C, respectively (see Fig. 2).

component frequencies as well as by spin splitting of the Landau levels. This latter effect will be discussed in more detail in Sec. IV D. Because the area of the largest cross section is important for an accurate determination of the shape of the surface as well as the volume enclosed, we have used a computer-programmed Fourier analysis to separate out the component frequencies. This has also been a helpful tool in many other orientations because of the complications exhibited by the data.

Figure 4 is the Fourier analysis of the data in Fig. 3. The peak at 3.96×10^5 G corresponds to the largest cross section of ellipsoid B. The peaks at 1.16 and 2.18×10^5 G correspond to the other two cross sections exhibited by ellipsoids A and C, respectively. In addition to these fundamental frequencies, a number of harmonics are also indicated. Figure 5 is a composite of the frequencies obtained from Fourier analyses of the data at all of the orientations measured. The solid circles represent the fundamental frequencies, while the open circles are harmonics of these. Not all the harmonics observed are plotted. For example, as many as five harmonics of the lowest-frequency branch corresponding to ellipsoid A were detectable. The solid curves in this figure were calculated from Eq. (4) for $K=13$ and $p=0.75\times10^{18}$ cm^{-3}.

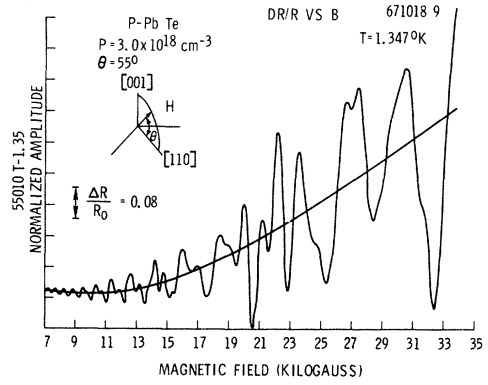

FIG. 3. Shubnikov–de Haas oscillations for the magnetic field orientation indicated in the figure. The center line is obtained from a least-squares fit of a low-order polynomial to the data. This center line is subtracted out before the data are Fourier analyzed in $1/H$.

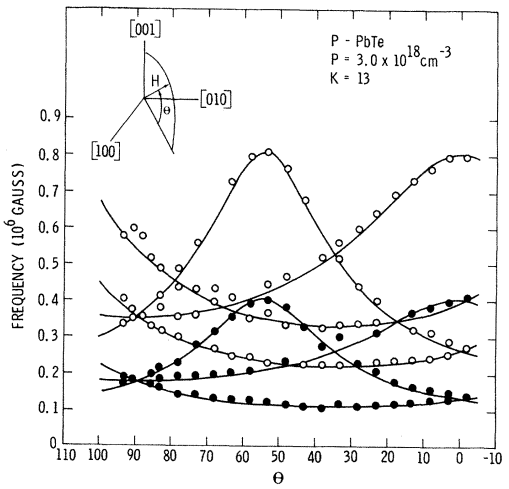

FIG. 5. Composite of the frequencies obtained from Fourier analyses of the data for each orientation of the magnetic field Θ measured. The solid circles represent fundamental frequencies, while the open circles are harmonics of these. Not all of the harmonics observed are plotted. As many as five harmonics of the lowest branch were detectable. The solid curves were obtained from Eq. (4) using $K=13$ and $p=0.75\times10^{18}$ cm^{-3}.

B. $\vec{k}\cdot\vec{p}$ Band Models

In a parabolic band, K is also the effective mass anisotropy. When the band is nonparabolic, however, the relationship between K and the mass anisotropy depends upon the specific dispersion relation.

Dimmock and Wright[10] (DW) first proposed a $\vec{k}\cdot\vec{p}$ band model for the lead salts that led to a dispersion relation which was a special case of the more general model previously derived for bismuth by Cohen.[8] This dispersion relation was originally applied to the lead salts by Cuff *et al.*[2,3] who used it to interpret the carrier-concentration dependence of the cyclotron effective mass. Although the DW model neglects the longitudinal interaction between conduction and valence bands that later theoretical work[12,13] showed to be important, the corresponding dispersion relation gives a useful description of the carrier-concentration dependence of the Fermi-surface parameters of PbTe. From Eq. (7) in DW, this relation is

$$(\hbar^2/m^2)P_\perp^2 k_\perp^2 = (\epsilon - \hbar^2 k_\parallel^2/2m_\parallel^v)(\epsilon + \epsilon_g + \hbar^2 k_\parallel^2/2m_\parallel^c), \tag{5}$$

where $\parallel$ and $\perp$ refer, respectively, to directions parallel and perpendicular to a $\langle 111\rangle$-type direction. $k_\parallel$ and $k_\perp$ are wave vectors; $m_\parallel^c$ and $m_\parallel^v$ are parabolic conduction and valence-band effective masses determined by next nearest bands; $P_\perp$ is the momentum matrix element describing the coupling of L-point conduction and valence-band states by the perpendicular component of the momentum operator; ϵ_g is the energy separation between L-point states, ϵ is the energy relative to the valence-band edge, and m is the free-electron mass. We can rewrite Eq. (5) in a form which more clearly shows its relationship to the ellipsoid-of-revolution parabolic model:

$$\frac{\hbar^2 k_\perp^2}{z\epsilon}\left[\frac{2P_\perp^2}{m^2\epsilon_g}\left(1+\frac{\epsilon}{\epsilon_g}+\frac{1}{\epsilon_g}\frac{\hbar^2 k_\parallel^2}{2m_\parallel^c}\right)^{-1}\right] + \frac{\hbar^2 k_\parallel^2}{2\epsilon}\frac{1}{m_\parallel^v} = 1 . \tag{6}$$

In view of the good agreement between Eq. (4) and the data shown in Fig. 5, we wish to consider expressions for extremal cross sections and cyclotron effective masses that are obtained from the ellipsoid-of-revolution approximation to Eq. (6). This approximation is obtained by neglecting the term $\hbar^2 k_\parallel^2/2m_\parallel^c$. For this case,

$$A_\perp = (2\pi/\hbar^2)[(m^2\epsilon_g/2P_\perp^2)m_\parallel^v]^{1/2}\epsilon(1+\epsilon/\epsilon_g)^{1/2} \tag{7}$$

where $A_\perp$ is the extremal cross section for $\vec{H}\perp$ [111]. Equation (15) of DW also shows that this is a good approximation to $A_\perp$ for the hole concentration of our sample. Without approximation,

$$A_\parallel = (2/\hbar^2)(m^2\epsilon_g/2P_\perp^2)\epsilon(1+\epsilon/\epsilon_g) , \tag{8}$$

where $A_\parallel$ is the extremal cross section for $\vec{H}\parallel$ [111].

The corresponding cyclotron effective masses can be obtained from the usual expression

$$m^{cyc} = (\hbar^2/2\pi)dA/d\epsilon . \tag{9}$$

Applying this to Eq. (8), we have

$$m_\parallel^{cyc} = (m^2\epsilon_g/2P_\perp^2)(1+2\epsilon/\epsilon_g) , \tag{10a}$$

$$m_\parallel^{cyc} = m_\parallel^{cyc}(0)(1+2\epsilon/\epsilon_g) , \tag{10b}$$

$$m_\parallel^{cyc} = m_\perp(0)(1+2\epsilon/\epsilon_g) , \tag{10c}$$

where $m_\parallel^{cyc}$ is the cyclotron effective mass for $\vec{H}\parallel$ [111] and $m_\parallel^{cyc}(0)$ is its band-edge value. Equation (10c) follows from Eq. (10b) for an ellipsoid of revolution for which $m_\perp(0)$ is the band-edge effective mass in all directions in a plane perpendicular to a $\langle 111\rangle$-type direction. Application of Eq. (9) to (7) yields

$$m_\perp^{cyc} = (m_\perp(0)m_\parallel^v)^{1/2}[1+\tfrac{3}{2}(\epsilon/\epsilon_g)](1+\epsilon/\epsilon_g)^{-1/2} , \tag{11}$$

where $m_\perp^{cyc}$ is the cyclotron effective mass for $\vec{H}\perp$ [111].

We have previously defined K to be the square of the maximum-to-minimum cross-section ratio of the ellipsoid. Therefore, making use of the definition of $m_\perp(0)$ made in Eqs. (10), the square of the ratio of Eq. (7) to Eq. (8) becomes

$$K = \frac{m_\parallel^v}{m_\perp(0)(1+\epsilon/\epsilon_g)} . \tag{12}$$

Thus, K is a measure of the *band-edge* mass anisotropy modified by the factor $(1+\epsilon/\epsilon_g)$. As Eq. (10c) shows, K is not, as one might expect, a measure of the mass anisotropy at the Fermi level. From Eqs. (10c) and (11),

$$\left(\frac{m_\perp^{cyc}}{m_\parallel^{cyc}}\right)^2 = \frac{m_\parallel^v}{m_\perp(0)(1+\epsilon/\epsilon_g)}\left[\frac{1+3/2(\epsilon/\epsilon_g)}{1+2(\epsilon/\epsilon_g)}\right]^2 . \tag{13}$$

This differs from K by the square of the energy factor in the brackets.

Figure 6 is a plot of K, normalized to its band-edge value $m_\parallel^v/m_\perp(0)$ versus the ratio of the Fermi energy to the energy gap. For the dispersion relation we have been discussing, the Fermi energy is related to the hole concentration by

$$p = 2^{9/2}\pi\{\nu^{2/3}[m_\perp^2(0)m_\parallel^v]^{1/3}\}^{3/2}/3h^3 \times \epsilon^{3/2}\left[1+\left(1+\frac{1}{5}\frac{m_\parallel^v}{m_\parallel^c}\right)\frac{\epsilon}{\epsilon_g}\right] \tag{14}$$

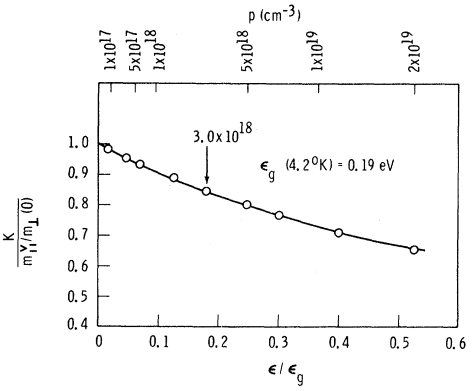

FIG. 6. K, normalized to its band-edge value, versus the ratio of the Fermi energy ϵ to the energy gap ϵ_g between conduction and valence bands for the DW model [see Eq. (12)]. The hole concentrations shown at the top of the figure were obtained from Eq. (14) for values of the parameters given in the text following that equation.

for degenerate statistics, where ν is the number of ellipsoids. Using $m_\perp(0) = 0.022$ eV (Ref. 3), $\epsilon_g = 0.19$ eV (Ref. 14), $m_\parallel^v = Km_\perp(0)$, and assuming $m_\parallel^v/m_\parallel^c = 1$, some values of p obtained from this equation are shown at the top of the figure. For $p = 3.0 \times 10^{18}$ cm^{-3}, ϵ is only about 12% smaller than the value obtained from the parabolic approximation to Eq. (14) (obtained by neglecting the energy term in square brackets). For the same p, the anisotropy K has decreased by only 15% of its band-edge value. Comparison of Eqs. (10c) and (12) shows that this decrease in K should be half of the corresponding decrease in the mass anisotropy $m_\parallel^v/m_\perp$.

Figure 7 shows the hole-concentration dependence of K (open circles) and $m_\perp/m$ (open triangles) reported by Cuff *et al.*[2] When $p = 3.0 \times 10^{18}$ cm^{-3}, K has decreased by about 50% of its band-edge value, approximately the same amount by which $m_\perp/m$ has increased. In contrast to this, the value of K we obtain for this concentration from the data in Fig. 5 is shown in Fig. 7 by the solid circle. The same value has recently been obtained by Schilz[7] from magnetoacoustic data for $p = 2.14 \times 10^{18}$ cm^{-3}.

As mentioned above, Cuff *et al.*[2,9] found that the number of holes contained in four ellipsoids with the K values they measured become less than the number measured by the high-field Hall coefficient as this latter number increased. To the contrary, for $p = 3.0 \times 10^{18}$ cm^{-3} we find excellent agreement between carrier counts obtained from these two methods. Since Cuff *et al.*[9] were able to account for all carriers at low concentrations using $K = 13$, our result suggests that K is constant at least up to $p = 3.0 \times 10^{18}$ cm^{-3}. The 15% decrease in K predicted by Eq. (12) is probably within our experimental error; however, we will consider briefly a more exact $\vec{k}\cdot\vec{p}$ band model and some approximations to it.

As discussed in detail by Mitchell and Wallis[13] and previously considered by Lin and Kleinman,[12] spin-orbit coupling in the lead salts leads to conduction- and valence-band wave functions at the L point which are coupled by both transverse and longitudinal momentum operators. Contrary to the DW model, one should therefore treat the longitudinal interaction in the exact solution of the $\vec{k}\cdot\vec{p}$ secular determinant rather than as a perturbation. This approach leads to the dispersion relation[15]

$$\frac{\hbar^2}{m^2}\{P_\perp^2 k_\perp^2 + P_\parallel^2 k_\parallel^2\} = (\epsilon - \hbar^2 k_\parallel^2/2m_\parallel^v - \hbar^2 k_\perp^2/2m_\perp^v) \times \left(\epsilon + \epsilon_g + \frac{\hbar^2 k_\parallel^2}{2m_\parallel^c} + \frac{\hbar^2 k_\perp^2}{2m_\perp^c}\right). \quad (15)$$

The principal departure from Eq. (5) is the addition of the term containing $P_\parallel^2$. Putting Eq. (15) into the form of Eq. (6) gives

$$\frac{\hbar^2 k_\perp^2}{2\epsilon}\left\{\frac{1}{m_\perp^v} + \frac{2P_\perp^2}{m^2\epsilon_g}\left[1 + \frac{\epsilon}{\epsilon_g} + \frac{1}{\epsilon_g}\left(\frac{\hbar^2 k_\parallel^2}{2m_\parallel^c} + \frac{\hbar^2 k_\perp^2}{2m_\perp^c}\right)\right]^{-1}\right\} + \frac{\hbar^2 k_\parallel^2}{2\epsilon}\left\{\frac{1}{m_\parallel^v} + \frac{2P_\parallel^2}{m^2\epsilon_g}\left[1 + \frac{\epsilon}{\epsilon_g} + \frac{1}{\epsilon_g}\left(\frac{\hbar^2 k_\parallel^2}{2m_\parallel^c} + \frac{\hbar^2 k_\perp^2}{2m_\perp^c}\right)\right]^{-1}\right\} = 1 . \quad (16)$$

As before, the nonellipsoidal terms will be neglected. If we can also neglect the terms $1/m_\parallel^v$ and $1/m_\perp^v$, which describe effective mass contributions by all bands other than the conduction band, Eq. (16) re-

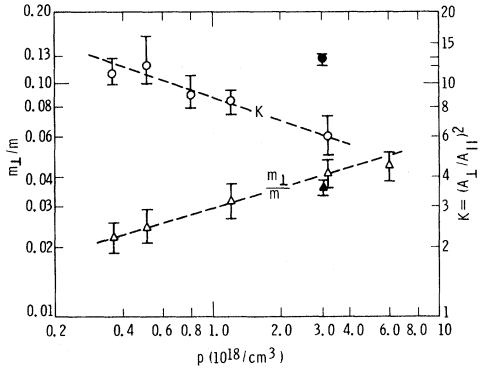

FIG. 7. Hole-concentration dependence of the "mass anisotropy" K (open circles) and the normalized transverse cyclotron mass $m_\perp/m$ (open triangles) reported by Cuff *et al.* (Ref. 2). The solid points correspond to our results for $P = 3.0 \times 10^{18}$ cm^{-3}. $A_\perp$ and $A_\parallel$ are, respectively, extremal cross sections of an ellipsoid for $\vec{H} \perp \langle 111 \rangle$ and $\vec{H} \parallel \langle 111 \rangle$ directions.

duces to the two-band model,

$$\frac{k_\perp^2}{(2\epsilon/\hbar^2)[m_\perp(0)(1+\epsilon/\epsilon_g)]} + \frac{k_\parallel^2}{(2\epsilon/\hbar^2)[m_\parallel(0)(1+\epsilon/\epsilon_g)]} = 1 \quad , \tag{17}$$

where $m_\parallel(0) = m^2\epsilon_g/2P_\parallel^2$ and as before, $m_\perp(0) = m^2\epsilon_g/2P_\perp^2$. The appealing feature of this relation is that

$$K = m_\parallel(0)/m_\perp(0) = (P_\perp/P_\parallel)^2 \quad , \tag{18}$$

i.e., it is independent of hole concentration.[16] We can also use Eq. (18) to obtain an estimate of $P_\parallel$, since $P_\perp$ can be computed from numbers available in the literature. It is conventional to calculate momentum matrix elements in units of energy. For $P_\perp$, we have

$$2P_\perp^2/m = m\epsilon_g/m_\perp(0) \quad . \tag{19}$$

Using $\epsilon_g = 0.19$ eV (Ref. 14) and $m_\perp(0) = 0.022m$ (Ref. 3), $2P_\perp^2/m = 8.6$ eV. This is larger than the value 6.4 eV reported by Cuff *et al.*[3] because of their use of an effective gap obtained from their measurements. Using 8.6 eV and Eq. (18), $2P_\parallel^2/m = 0.66$ eV for $K = 13$.

Application of Eq. (9) to the extremal areas obtained from Eq. (17) shows that

$$K = (m_\perp^{cyc}/m_\parallel^{cyc})^2 \quad . \tag{20}$$

Since this differs from the relationship between these quantities described by Eqs. (12) and (13), one could also hope to see the difference between the models described by Eqs. (6) and (17) in measurements of cross-section and cyclotron mass anisotropies. However, this may not be practical in the lead salts where precision cyclotron mass measurements are difficult, for reasons described in Sec. IV C.

C. Effective Mass

From Eqs. (1) and (2), the amplitude of the oscillation at the fundamental frequency ($r = 1$) at temperature T_1 is related to that at temperature T_2 by

$$\frac{A(T_1)}{A(T_2)} = \frac{T_1 \sinh(2\pi^2 kT_2/\hbar\omega_c)}{T_2 \sinh(2\pi^2 kT_1/\hbar\omega_c)} \quad , \tag{21}$$

where $\omega_c = eH/m^{cyc}c$. For small values of $\hbar\omega_c$, the ratio of sinh functions can be approximated by an exponential. m^{cyc} can then be determined from the slope of a semilog plot of $A(T_1)/A(T_2)$ versus $1/H$. The cyclotron mass and collision broadening of the Landau levels in PbTe are such that the exact form of Eq. (21) is necessary at most fields at which oscillations can be observed. We have obtained m^{cyc} from a least-squares fit of Eq. (21) to amplitude ratios obtained for several different values of $1/H$. An average cyclotron mass was obtained by doing this at a number of different temperatures.

Figure 8 shows the oscillations for $\vec{H} \parallel [111]$, with $T_1 = 3.19$ °K and $T_2 = 1.36$ °K. Data for the least-squares analysis were obtained from the envelope of these curves and restricted to the field range in which only the fundamental frequency from one ellipsoid (ellipsoid A in Fig. 2) was present.

Figure 9 shows the dependence of the amplitude ratio on $1/H$. The data are indicated by the circles, and the bars are a measure of their uncertainty. The X's are calculated amplitude ratios for the best-fit value of m^{cyc} indicated in the figure.

The second column of Table I gives the average of the best-fit m^{cyc}/m values for $\vec{H} \parallel [111]$ and [001]. The uncertainties are defined by the scatter of the best-fit masses obtained from several sets of temperature differences. m^{cyc}/m for $\vec{H} \parallel [111]$ is in good agreement with that previously reported by Cuff *et al.*[2] for material having approximately the same hole concentration (see Fig. 7). The percentage uncertainty in m^{cyc}/m for $\vec{H} \parallel [001]$ is about three times as large as that for $\vec{H} \parallel [111]$. This was surprising because the [001] data were of higher quality and were obtained over a larger field range before interference by the second har-

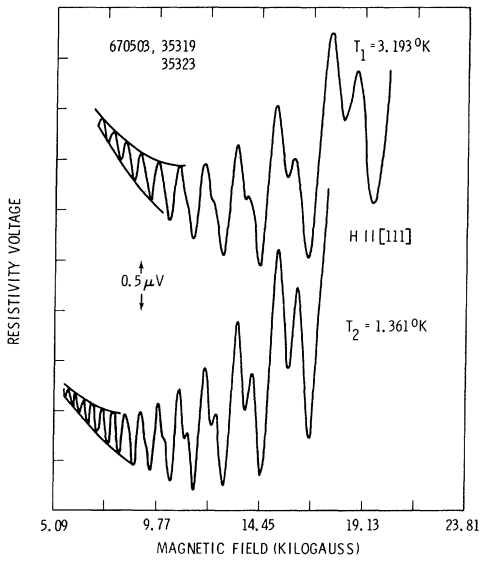

FIG. 8. Temperature dependence of the amplitude of the oscillatory component of the resistivity voltage for $\vec{H} \parallel [111]$. In this field range, the data are generated by ellipsoid A (Fig. 2), and consist of the fundamental frequency and its second harmonic. The doubling of the peaks is due to spin splitting of the Landau levels.

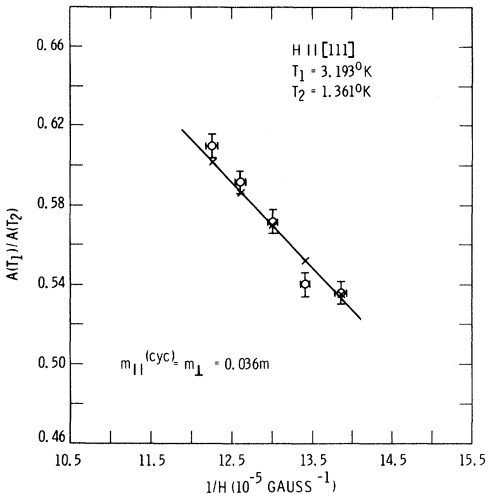

FIG. 9. $1/H$ dependence of the amplitude ratios obtained from the data in Fig. 8. The x's are ratios calculated from Eq. (21) for $m_\perp = 0.036m$, the "best" mass obtained from the least-squares fit.

monic became observable. However, since the cyclotron masses of the ellipsoids are degenerate for $\vec{H} \parallel [001]$, a small misorientation would lead to four slightly different temperature dependences, the average value of which would depend on the temperature interval chosen. Because of this uncertainty, we are not able to make the comparison between cross-section and cyclotron mass anisotropies described in the Sec. IV B. For this purpose, it is now clear that a choice other than $\vec{H} \parallel \langle 001 \rangle$-type directions is preferable. Most desirable of course is a measurement for $\vec{H} \perp \langle 111 \rangle$-type directions. However, interference by other frequencies as well as harmonics (see Fig. 5) makes this a difficult matter for this as well as most other orientations.

Table I also includes ratios of spin splitting to Landau-level separation $m^{cyc}g/2m$ and effective g values which will now be discussed.

D. Effective g Value

The effective g value is defined in terms of the energy that spin contributes to the total electronic energy

$$\epsilon_{n\pm} = (n + \tfrac{1}{2})\hbar\omega_c(\epsilon) \pm \tfrac{1}{2}g(\epsilon)\beta_0 H \qquad (22)$$

in a magnetic field H. As Fig. 10 shows, $\hbar\omega_c(\epsilon)$ is the energy separation between Landau states n and $n-1$. The former, for example, is split into spin-down and spin-up states, $n+$ and $n-$, respectively, separated in energy by $g(\epsilon)\beta_0 H$, where $g(\epsilon)$ is the effective g value and β_0 is the Bohr magneton. Both the cyclotron frequency $\omega_c(\epsilon)$

TABLE I. Normalized cyclotron effective masses m^{cyc}/m, ratios of spin splitting to Landau-level separation $m^{cyc}g/2m$, and effective g values for magnetic fields parallel to [111], [001], and [110] directions. The [111] values are for ellipsoid A in Fig. 2, and the [110] values are for ellipsoids C.

Field direction	m^{cyc}/m	$m^{cyc}g/2m$	g
[111]	0.036 ± 0.002	0.58 ± 0.01	32 ± 2
[001]	0.051 ± 0.008	0.58 ± 0.01	23 ± 5
[110]	0.080 ± 0.014[a]	0.27 ± 0.01	7 ± 2

[a]Calculated value [see Eq. (28)].

and the effective g value $g(\epsilon)$ will be a function of ϵ, the energy relative to the band edge, when the band of interest interacts strongly with other bands.[17]

For values of $1/H$ and n for which the right-hand side of Eq. (22) is equal to the Fermi energy ϵ_F, one can show that

$$\frac{(1/H)_{n+} - (1/H)_{n-}}{(1/H)_{n+} - (1/H)_{(n-1)+}} = \frac{m^{cyc}(\epsilon_F)g(\epsilon_F)}{2m} \quad , \qquad (23)$$

where, for example, $(1/H)_{n+}$ means the value of $1/H$ for which the energy of the state $n+$ is equal to ϵ_F. For sufficiently high magnetic fields, these differences in $1/H$ can be directly determined by the separation in the corresponding peaks of the Shubnikov–de Haas oscillations. One only needs to make the correct association of these peaks with the levels shown in Fig. 10. Here a knowledge of the phase of the oscillations is helpful. The cosine function in Eq. (1) can be written

$$\cos(2\pi F/H - \phi) \quad , \qquad (24a)$$

where the frequency is

$$F = rc\hbar S/2\pi e \quad , \qquad (24b)$$

and the phase is

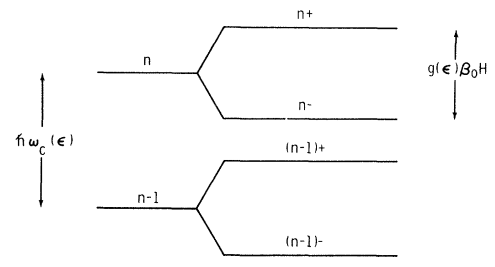

FIG. 10. Splitting of the Landau levels n and $n-1$ into spin-down (+) and spin-up (−) states. $\omega_c(\epsilon)$ is the cyclotron frequency, $g(\epsilon)$ is the effective g value, and β_0 is the Bohr magneton.

$$\phi = 2\pi r\gamma + \tfrac{1}{4}\pi + \delta \quad . \tag{24c}$$

When γ is assumed to be $\frac{1}{2}$, the term $2\pi r\gamma$ is omitted from the phase, and the factor $(-1)^r$ is introduced in front of Eq. (2). The phase shift δ, which is either zero or π, is determined by the function $\cos(\pi m^{cyc} rg/2m)$ in Eq. (2) and thus is influenced by the size of the g value. From Eq. (24a), the conditions for extrema in a component oscillation are

$$\begin{aligned} &F/H - \phi/2\pi = m, \quad \text{maxima} \ , \\ &F/H - \phi/2\pi = m + \tfrac{1}{2}, \quad \text{minima} \ , \end{aligned} \tag{25}$$

where m is an integer. Using a plot of integral multiples of one-half versus the $1/H$ values of the extrema, we can decide which values of m lead to a value of $\phi/2\pi$ which agrees best with that calculated from Eq. (24c) for $\delta = 0$ or π. This analysis is described by Figs. 11 and 12 for the fundamental component ($r = 1$). The solid curve in Fig. 11 is a datum for $\vec{H} \parallel [001]$. Fourier analysis (Fig. 13) shows that it consists essentially of the fundamental frequency and its second harmonic. The positions of the maxima and minima of the fundamental component in the high-field region were obtained from the extrapolation indicated by the dashed curve. This extrapolation was made subject to the restrictions that (i) the fundamental component have the same frequency as the low-field data and as given by the Fourier analysis, and (ii) the intersections of the dashed curve with the data give the correct separation between zeros of the second harmonic component. Figure 12 is a plot of the $1/H$ positions of the maxima and minima of the dashed curve. Labeling the ordinate to obtain an intercept which best agrees with Eq. (24c), one obtains $\delta = \pi$ and $\gamma = 0.67 \pm 0.05$. A generalized derivation of γ, given by Roth,[18] shows a magnetic field dependence which leads to values other than $\frac{1}{2}$. Although our value does differ from $\frac{1}{2}$, there is neither nonlinearity in Fig. 12, nor differences in the frequencies obtained from Fourier analyses over different field ranges to suggest that it is magnetic field dependent.

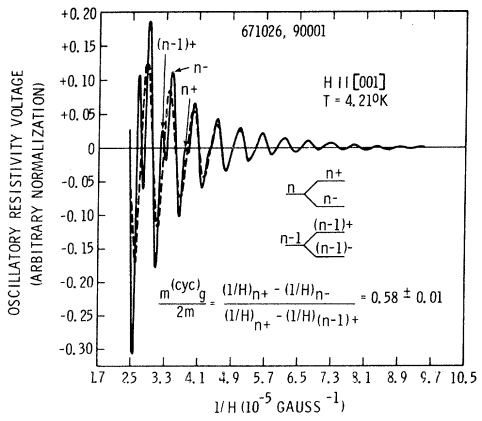

FIG. 11. Normalized oscillatory component of the resistivity versus $1/H$. The solid curve is composed of the fundamental frequency and its second harmonic. The doubling of the peaks is due to spin splitting of the Landau levels. The dashed curve is an extrapolation (see text) of the fundamental component. The assignment of peaks in the oscillations to the energy levels shown is consistent with the result that $m^{cyc}g/2m > \frac{1}{2}$.

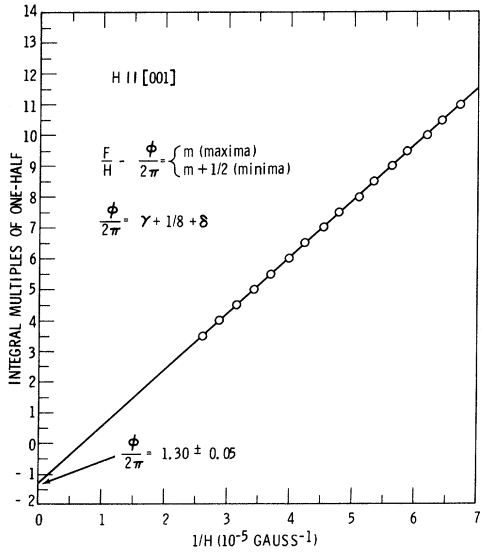

FIG. 12. Integral multiples of one-half versus the $1/H$ values of the maxima and minima of the dashed curve in Fig. 11. Assuming γ is close to $\frac{1}{2}$, its "free-electron" value, and labeling the ordinate to obtain an intercept which best agrees with Eq. (24c), $\delta = \pi$, and $\gamma = 0.67 \pm 0.05$.

For $\delta = \pi$, $\cos(\pi m^{cyc} g/2m)$ is negative and $m^{cyc}g/2m > 0.5$. Figure 11 shows an assignment of the energy levels to the peaks in the solid curve that is consistent with this result. This assignment is is not unique but gives the smallest acceptable value of $m^{cyc}g/2m$. Using Eq. (22) and the peaks indicated, one obtains

$$m^{cyc}(\epsilon_F) g(\epsilon_F)/2m = 0.58 \pm 0.01 \quad . \tag{26}$$

A similar analysis performed on the data in Fig. 8 gave the same result within experimental error. Table I gives the g values that are obtained for these two orientations from Eq. (26) and the average values of the corresponding cyclotron masses. The value $g_{\parallel}(\epsilon_F) = 32 \pm 2$ is to be compared with the band-edge value of 51 ± 8 reported by Cuff *et al.*[3] Schilz[7] has reported $g_{\parallel}(\epsilon_F) = 36 \pm 2$ for $p = 4 \times 10^{18}$ cm^{-3}. However, as he points out in a note added in proof, a different assignment of spin levels to

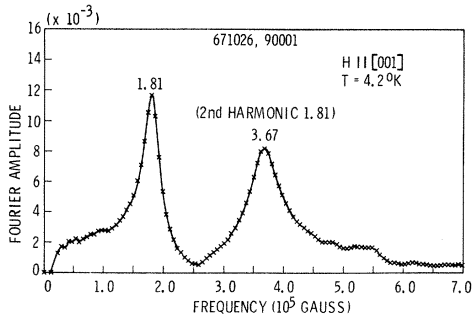

FIG. 13. Fourier analysis of the data in Fig. 11 showing that it consists almost completely of the fundamental frequency at 1.81×10^5 G and its second harmonic at 3.6 $\times10^5$ G.

the peaks in the magnetoacoustic oscillations should have been made. His new assignment agrees with that presented here. He also used the band-edge effective mass reported by Cuff *et al.*[3] to compute $g_{\parallel}(\epsilon_F)$ rather than the mass at the Fermi level. When both corrections are made, his value agrees with ours. When similar corrections are made to his value of $g_{\parallel}(\epsilon_F)$ for $p=6\times10^{18}$ cm^{-3}, the corrected value is smaller, rather than larger, than the corrected value for $p=4\times10^{18}$ cm^{-3}. These corrected results, as well as that presented here, are then consistent with a smooth increase of $g_{\parallel}$ to the band-edge value reported by Cuff *et al.*[3]

Effective g values for the lead salts have also been obtained from magnetoemission studies in p-n junctions by Butler and Calawa,[19] and for n-type PbTe from spin-flip Raman scattering by Patel and Slusher.[20] The magnetoemission experiment measures a g value that is a combination of its conduction- and valence-band values g^c and g^v, respectively. Assuming $|g^v|=|g^c|$, as magnetoabsorption studies[14] have suggested, Butler and Calawa[19] obtain $g=29$ for $\vec{H}\parallel[001]$ for both bands. As they expect this to be approximately a band-edge value, it is reasonable for it to be somewhat larger than our value given in Table I.

In one of the more direct experiments for obtaining g values of free electrons, Patel and Slusher[20] found $g_{\parallel}^c=57\pm2$ and $g_{\perp}^c=15\pm1$ for the conduction band of PbTe. These are also approximately band-edge values since their material has electron concentrations between 8 and 10×10^{16} cm^{-3}. If we assume $|g^v|=|g^c|$, $g_{\parallel}^c=57\pm2$ is within the uncertainty range quoted by Cuff *et al.*[3] for the band-edge value of $g_{\parallel}^v$. However, it is significantly different from their value for the conduction-band edge. Table II summarizes these g values and, in addition, includes our value of $g_{\perp}^v$ obtained from data to be described below.

The two-band analysis of PbTe by DW[10] showed that $m^{cyc}g/2m=1$ for $\vec{H}\parallel[111]$, independent of carrier concentration. This is a result previously reported by Cohen for bismuth and of general validity in a two-band model. Our value of 0.58 $\pm$0.01 for $m_{\parallel}^{cyc}g_{\parallel}/2m$ shows that there is a transverse momentum operator $P_{\perp}'$ coupling the valence band to a second conduction band. This coupling was neglected when the term $1/m_{\perp}^v$ was dropped from Eq. (16). (Reference 16 shows that K is independent of carrier concentration for less restrictive approximations.) However, this approximation was not necessarily unreasonable, because contributions from other bands often affect g values to a greater extent than effective masses (see Ref. 13). DW[10] have given an expression for $m_{\parallel}^{cyc}g_{\parallel}/2m$ in a three-band model. For small ϵ they obtain

$$m_{\parallel}^{cyc}g_{\parallel}/2m=\pm(\epsilon_c'-\epsilon_g)/(\epsilon_c'+\epsilon_g)\ , \qquad (27)$$

where $\epsilon_c'=\epsilon_c P_{\perp}^2/P_{\perp}'^2$, and ϵ_c is the energy gap between the valence and second conduction bands. Thus, using 0.58 for $m_{\parallel}^{cyc}g_{\parallel}/2m$ and 0.19 eV for ϵ_g, one obtains $\epsilon_c'=0.72$ eV. Letting $\epsilon_c=\Delta1=1.3$ eV, the energy gap between the valence and second conduction bands calculated by Lin and Kleinman,[12] we find $P_{\perp}'^2/2m=15.6$ eV. This is larger than the value 8.6 eV obtained for $P_{\perp}^2/2m$ from Eq. (19).

Roth[21] has shown that $g_{\perp}$, the effective g value for H perpendicular to the major axis of an ellipsoid of revolution, will differ from the free-electron value of 2 *only* if the band in question is coupled to another band by $P_{\perp}$ and $P_{\parallel}$. Thus, a measurement of $g_{\perp}$ is a sensitive test for the presence of both interactions. It is usually difficult to detect spin splitting in the Shubnikov–de Haas oscillations corresponding to the largest extremal orbit because of damping by the correspondingly large cyclotron mass. However, with the use of fields up to 150 kG, we believe we have been able

TABLE II. Summary of experimental effective g values for the valence and conduction bands of PbTe.

Band	Authors	Carrier concentration (cm^{-3})	$g_{\parallel}$	$g_{\perp}$	g[001]
Valence	Cuff *et al.*	0	51 $\pm$ 8		
	Butler and Calawa	p-n junction			29[b]
	Burke *et al.*	3×10^{18}	32 $\pm$ 2	7 $\pm$ 2	23 $\pm$ 5
	Schilz	4×10^{18}	36(32)[a] $\pm$ 2		
		6×10^{18}	45(22)[a] $\pm$ 2		
Conduction	Cuff *et al.*	0	45 $\pm$ 8		
	Patel and Slusher	$8-10\times10^{16}$	57 $\pm$ 2	15 $\pm$ 1	35[c]
	Butler and Calawa	p-n junction			29[b]

[a] Numbers in parenthesis are corrected values (see text).
[b] Obtained by assuming $|g^v|=|g^c|$.
[c] Calculated from $g_\theta=(g_{\parallel}^2\cos^2\Theta+g_{\perp}^2\sin^2\Theta)^{1/2}$, where Θ is the angle between the magnetic field and a $\langle111\rangle$-type direction.

to see it. Figure 14 shows data for $\vec{H} \parallel [110]$ in which only two fundamental frequencies should be present. One corresponds to ellipsoids A and B, while the other is generated by the largest extremal orbit of ellipsoids C (see Fig. 2). Figure 15 is the Fourier analysis of this data. Although the peak at 4.09×10^5 G occurs almost precisely at a frequency three times that of the fundamental at 1.4×10^5 G, two reasons for associating it with the largest extremal orbit of ellipsoids C are (i) Its amplitude is larger than that of the fundamental at 1.4×10^5 G, and (ii) as Fig. 5 shows, its frequency is the same as the maximum value obtained at $\Theta = 55°$, where it is no longer degenerate with the third harmonic of the lowest branch. Perhaps the best evidence for this choice can be obtained from Fig. 16, which is a plot of integers versus the $1/H$ values of the maxima of the high-frequency component in Fig. 14. According to Eq. (24c) the intercept at $1/H = 0$ will depend on whether this component is a fundamental ($r = 1$) or a third harmonic ($r = 3$). The value $(\phi/2\pi)_{\text{calc}} = 0.80$ is obtained for the parameters $r = 1$, $\delta = 0$, and, as determined above, $\gamma = 0.67$. The intercept, for the choice of integers shown, is in good agreement with $(\phi/2\pi)_{\text{calc}}$ and is unique in the sense that this agreement is much better than that which can be obtained for $r = 3$ and/or $\delta = \pi$.

For $\delta = 0$, $\cos(\pi m_\perp^{\text{cyc}} g_\perp / 2m)$ is positive and $m_\perp^{\text{cyc}} g_\perp / 2m < \frac{1}{2}$. The peak splitting consistent with this is indicated by the two dashed arrows in Fig. 14. Using Eq. (23), we find

$$m_\perp^{\text{cyc}} g_\perp / 2m = 0.27 \pm 0.01 \ . \tag{28}$$

From either Eqs. (11) and (12) or (18) and (20) for the hole concentration of our sample, we find

$$m_\perp^{\text{cyc}} \simeq [m_\perp^2(0) K]^{1/2} \ . \tag{29}$$

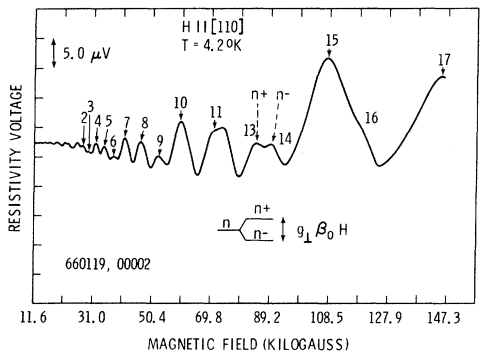

FIG. 14. High-field oscillations for $\vec{H} \parallel [110]$. The peaks indicated by $n+$ and $n-$ are associated with the spin splitting $g_\perp \beta_0 H$ of the Landau levels of the carriers in ellipsoids C in Fig. 2. The numbered maxima correspond to the numbered points shown in Fig. 16.

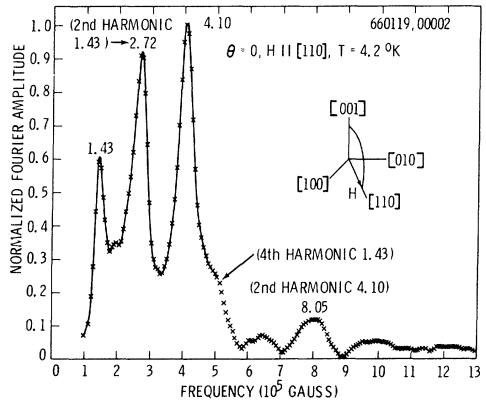

FIG. 15. Fourier analysis of the data in Fig. 14. We associate the peak at 4.10×10^5 G with the largest extremal orbit of ellipsoid C in Fig. 2.

Thus, for $m_\perp(0)/m = 0.022 \pm 0.003$ (Ref. 3) and $K = 13 \pm 1$, one obtains

$$m_\perp^{\text{cyc}}/m = 0.080 \pm 0.014 \quad \text{and} \quad g_\perp = 7 \pm 2 \ . \tag{30}$$

As discussed above, this deviation of $g_\perp$ from its free-electron value is evidence that the conduction and valence bands are coupled by longitudinal as well as transverse momentum operators. If we assume $|g_\perp^v| = |g_\perp^c|$, our Fermi-level value for $g_\perp^v$ is smaller and therefore consistent with the band-edge value of $g_\perp^c$ obtained by Patel and Slusher.[20]

V. SUMMARY AND CONCLUSIONS

We have studied the angular dependence of Shubnikov–de Haas oscillations in a sample of p-type PbTe having a hole concentration of 3.0×10^{18} cm^{-3}. For the first time in this material, the component frequencies were determined by Fourier analysis. The angular dependence of these frequencies corresponds to a prolate ellipsoidal ⟨111⟩ surface having an anisotropy $K = 13$. Four ⟨111⟩ surfaces with this anisotropy generated a volume in k space which precisely accounts for the number of holes determined from the high-field Hall coefficient. These results are considerably different than those obtained by Cuff, Ellett, and Kuglin for this hole concentration. They reported $K \simeq 6$, and were unable to account for all carriers. We believe their results differ from ours principally because of the better resolution that can be obtained through Fourier analysis and the use of larger magnetic fields. The presence of higher harmonics, enhanced by spin splitting of the Landau levels, together with heavy damping of the frequencies contributed by the large extremal areas, make these areas very difficult to determine by conventional analysis. This is especially true at higher carrier concentrations.

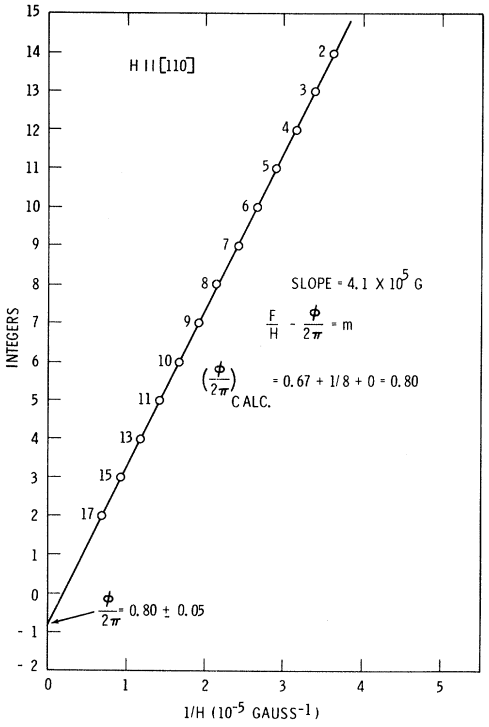

FIG. 16. Integers versus the $1/H$ values of the maxima in Fig. 14. The numbered points correspond to the numbered maxima in Fig. 14. The slope F of the line is in good agreement with the peak at 4.10×10^5 G in Fig. 15. $(\phi/2\pi)_{\text{calc}}$ is obtained by assuming F is a fundamental frequency.

Since K, measured by Cuff *et al.* for hole concentrations in the low 10^{17}-cm^{-3} range, was also approximately 13, one feels that K is probably independent of hole concentration, at least up to $p = 3.0 \times 10^{18}$ cm^{-3}. Theoretical work by Lin and Kleinman and by Mitchell and Wallis shows that the longitudinal coupling between conduction and valence bands cannot be neglected as in the DW model. When this interaction is included in the $\vec{k}\cdot\vec{p}$ secular determinant and reasonable approximations to the resulting dispersion relations are made, one obtains an expression for an ellipsoid of revolution in which K is a constant, independent of carrier concentration.

For $\vec{H} \parallel [111]$, the ratio of spin splitting to Landau-level separation $m^{\text{cyc}}(\epsilon_F)g(\epsilon_F)/2m$ is 0.58 ± 0.01. This deviation from the value 1 for a two-band model shows that there is a transverse momentum operator coupling the valence band to a second conduction band. Using the corresponding cyclotron effective mass gives $g_{\parallel}(\epsilon_F) = 32 \pm 2$. In fields greater than about 70 kG, we believe we have observed spin splitting in the Shubnikov–de Haas oscillations corresponding to the largest extremal orbit on the ellipsoid. From this splitting we obtain $g_{\perp}(\epsilon_F) = 7 \pm 2$. This deviation of $g_{\perp}$ from the free-electron value of 2 is evidence that the valence band is coupled to the primary conduction band by longitudinal as well as transverse momentum operators.

ACKNOWLEDGMENTS

The authors wish to acknowledge their collaboration with Dr. J. Babiskin and P. G. Siebenmann of the Naval Research Laboratory in the early stages of this work. Several discussions with Dr. P. J. Lin and Dr. D. L. Mitchell, also of the Naval Research Laboratory, concerning the $\vec{k}\cdot\vec{p}$ method and g values in the lead salts, were invaluable. We are indebted to Dr. J. O. Dimmock of the M.I.T. Lincoln Laboratory for pointing out other ellipsoidal nonparabolic band models which are consistent with our data. Dr. K. F. Cuff of Lockheed Research Laboratories and Dr. W. Schilz of Philips Zentrallaboratorium communicated to us unpublished data on PbTe. These data were very helpful and are greatly appreciated. Finally, we wish to thank Dr. R. S. Allgaier of this Laboratory for his review of the manuscript.

[1]For a review of work on PbTe see J. R. Burke, Jr., Phys. Rev. 160, 636 (1967).

[2]K. F. Cuff, M. R. Ellett, and C. D. Kuglin, in *Proceedings of the International Conference on the Physics of Semiconductors, Exeter*, 1962 (Institute of Physics and Physical Society, London, 1962), p. 316.

[3]K. F. Cuff, M. R. Ellett, C. D. Kuglin, and L. R. Williams, in *Proceedings of the International Conference on the Physics of Semiconductors, Paris*, 1964 (Dunod, Paris, 1964), p. 677.

[4]J. R. Burke, B. Houston, H. T. Savage, J. Babiskin, and P. G. Siebenmann, Bull. Am. Phys. Soc. 13, 484 (1968).

[5]P. J. Stiles, E. Burstein, and D. N. Langenberg, J. Appl. Phys. 32, 2174 (1961).

[6]R. Nii, J. Phys. Soc. Japan 19, 58 (1964).

[7]W. Schilz, J. Phys. Chem. Solids 30, 893 (1969).

[8]M. H. Cohen, Phys. Rev. 121, 387 (1961).

[9]K. F. Cuff (private communication).

[10]J. O. Dimmock and G. B. Wright, Phys. Rev. 135, A821 (1964).

[11]For a review of this work see L. M. Roth and P. N. Argyres, in *Semiconductors and Semimetals*, edited by R. K. Willardson and A. C. Beer (Academic, New York, 1966), Vol. 1, p. 159.

[12]P. J. Lin and L. Kleinman, Phys. Rev. 142, 478 (1966).

[13]D. L. Mitchell and R. F. Wallis, Phys. Rev. 151, 581 (1966).

[14]D. L. Mitchell, E. D. Palik, and J. N. Zemel, in

Ref. 3, p. 325.

[15]P. J. Lin and D. L. Mitchell (private communication). This dispersion relation has also been used by G. A. Antcliffe.

[16]J. O. Dimmock has pointed out that there are less restrictive approximations than we have made to Eqs. (15) or (16) which also yield an ellipsoidal model with $K=(P_\perp/P_\parallel)^2$. The most general of these is obtained by setting $P_\perp^2/P_\parallel^2=m_\parallel^v/m_\perp^v=m_\parallel^c/m_\perp^c$.

[17]B. Lax, J. G. Mavroides, H. J. Zeiger, and R. J. Keyes, Phys. Rev. 122, 31 (1961).

[18]L. M. Roth, Phys. Rev. 145, 434 (1966).

[19]J. F. Butler and A. R. Calawa, in *Physics of Quantum Electronics*, edited by P. L. Kelley, B. Lax, and P. E. Tannenwald (McGraw-Hill, New York, 1966), pp. 458-466.

[20]C. K. N. Patel and R. E. Slusher, Phys. Rev. 177, 1200 (1969).

[21]L. M. Roth, Phys. Rev. 118, 1534 (1960).

PHYSICAL REVIEW B VOLUME 2, NUMBER 6 15 SEPTEMBER 1970

Luminescence and Minority Carrier Recombination in p-Type GaP(Zn,O)

J. M. Dishman, M. DiDomenico, Jr., and R. Caruso

Bell Telephone Laboratories, Murray Hill, New Jersey 07974

(Received 16 April 1970)

A detailed study of luminescence and minority carrier recombination in Zn- and O-doped p-GaP is presented. To interpret the results of photoluminescence measurements, a three-path model for minority carrier recombination is developed. This model includes recombination through nearest-neighbor Zn-O complexes, isolated O donors, and an unspecified shunt path. Included in the model are the effects of thermalization of electrons trapped on Zn-O centers and the effects of plasma screening by free holes on excitons bound to these centers. These processes together with nonradiative Auger recombination of excitons and trapped electrons at Zn-O complexes provide the major limitation of the red quantum efficiency in GaP-(Zn, O). Using an iterative self-consistent fit to the available temperature and Zn-doping dependence of the red luminescence efficiency and time decay, values are obtained for all of the important capture cross sections, time decay parameters, and Auger recombination coefficients, as well as the minority carrier lifetime. In addition, the concentrations of the deep Zn-O and O centers are measured optically. It is concluded that the bulk quantum efficiency of GaP(Zn,O) can be improved by simultaneously increasing the minority carrier lifetime and decreasing the free-hole concentration (and consequent Auger processes) by compensation.

I. INTRODUCTION

Two deep radiative recombination centers are introduced into GaP by the simultaneous presence of zinc and oxygen impurities. Isolated oxygen is a deep donor approximately 0.9 eV below the conduction band.[1] Infrared radiative recombination at oxygen ($h\nu \approx 1.35$ eV) occurs when trapped electrons recombine either with holes trapped on isolated zinc acceptors[1] or with free holes.[2] The isoelectronic center formed by a zinc acceptor and an oxygen donor on nearest-neighbor sites (Zn-O complex) also acts as a deep electron trap approximately 0.2–0.3 eV below the conduction band.[3,4] Red luminescence ($h\nu \approx 1.77$ eV) originates from Zn-O centers in two ways: (i) by pair recombination of trapped electrons with holes on distant Zn acceptors and (ii) by recombination of bound excitons. At room temperature, the red luminescence is essentially excitonic,[4] whereas the infrared luminescence is essentially free to bound.[2]

In a previous paper[5] (hereafter referred to as I), a general model for the recombination kinetics of electrons and holes at isoelectronic centers was developed. This model considered in detail the three occupation states of the isoelectronic center, i.e., empty, electron (hole) occupied, and exciton occupied. It therefore generalized the conventional two-state Shockley-Read-Hall[6] (SRH) recombination model applicable to nonisoelectronic centers. In the present paper we study minority carrier recombination in p-type Zn- and O-doped GaP by photoluminescence techniques. A three-path model for the minority carrier recombination in presented.[7] This model includes recombination through the isoelectronic Zn-O complex, the deep O donor, and an unspecified "shunt path" which accounts for all other nonradiative centers. The results derived in I are applied in describing recombination through the Zn-O luminescent center. In this treatment we also consider explicitly how the recombination mechanisms associated with the Zn-O center are modified